# Ⅲ-4

## Surface, Interface and Thin Films

Highlight

BL5U

# Polarization-dependent Photoelectron Intensity in Ca-doped Graphene

S. Ichinokura[1], K. Tokuda[1], K. Tanaka[2] and T. Hirahara[1]
[1]*Department of Physics, Tokyo Institute of Technology, Tokyo 152-8551, Japan*
[2]*UVSOR Facility, Institute for Molecular Science, Okazaki 444-8585, Japan*

Orbital symmetry strongly influences the interaction between light and electrons. When polarized light is irradiated on a material, the electronic excitation obeys the dipole selection rule; electrons in orbitals with odd- and even-parity are excited by *s*- and *p*-polarized light (described as *s*- and *p*-pol. hereafter), respectively. Therefore, in angle-resolved photoemission spectroscopy (ARPES), complemental intensity maps will be obtained when the *s*- and *p*-linear polarized lights are used.

The remarkable high-carrier mobility in graphene originates from its characteristic π-orbital band called Dirac cone. The light-matter interaction of graphene through the π-electron has attracted considerable attention. For example, the photoelectron intensity of the Dirac electronic state varies cyclically on the $k_x$-$k_y$ plane for the polarized light [1]. Here, chirality plays an essential role in polarization dependence. In Li-intercalated bilayer graphene ($C_6LiC_6$), two Dirac cones with different chirality overlap around the Γ point of the Brillouin zone (BZ). The chiral symmetry is broken due to the lattice distortion by Li, leading to the gap opening at the Dirac point. These properties were clarified by laser-ARPES measurements [2].

Ca-intercalated graphite and graphene become superconducting at relatively high temperatures in layered and two-dimensional materials [3-5]. In addition to the Dirac cones, a free-electron-like state called interlayer band (ILB) exists as an occupied state in those systems. Since ILB has different symmetry from π-band, dipole selection rule and chirality effects are expected to coexist in $C_6CaC_6$.

To resolve the coexistence of the two effects, we performed high-resolution polarization-dependent ARPES measurements on Ca-intercalated bilayer graphene, $C_6CaC_6$ at BL5U and BL7U. As shown in Figure 1(a), $C_6CaC_6$ was prepared on a Ca-terminated SiC substrate. Figure 1(b) shows the ARPES spectrum obtained by *s*-pol. A double Dirac cone was seen. The Dirac cones are folded into Γ point from K point of the graphene's BZ due to the $\sqrt{3}\times\sqrt{3}$ periodicity of Ca. The doubling is caused by the interlayer interaction between two graphene layers.

On the other hand, a parabolic band (stressed by dashed line) was much more prominently observed than the double Dirac cones when *p*-pol. is used, as shown in Figure 1(c). The free-electron-like character is consistent with the ILB. Since the spectrum by *p*-pol. and *s*-pol. are complementary, dipole selection rule mainly determines the intensity distribution; odd- and even-parity components are excited by *s*- and *p*-polarization, respectively.

Figures 1(d) and 1(e) show the photoelectron intensity maps on the Fermi energy obtained for *s*- and *p*-polarized light. In Fig. 1(d), the photoelectron intensity has an anisotropy; intensity map along Γ-K and Γ-K' direction (shown by dashed lines) is not identical. On the other hand, in Fig. 1(e), the intensity distribution is almost isotropic. Since the Dirac state is mainly excited by *s*-pol., the anisotropy is estimated to be caused by chirality effect.

In conclusion, it was revealed that the dipole selection rule has a stronger effect on the intensity distribution of photoelectron in $C_6CaC_6$ than the chirality effect. Reflecting the different symmetry of π-bands and ILB, complementary distribution was observed in the Fermi contour for the *s*- and *p*-polarized light. The chirality effect appears as the anisotropy in the Fermi contour of the Dirac cone component.

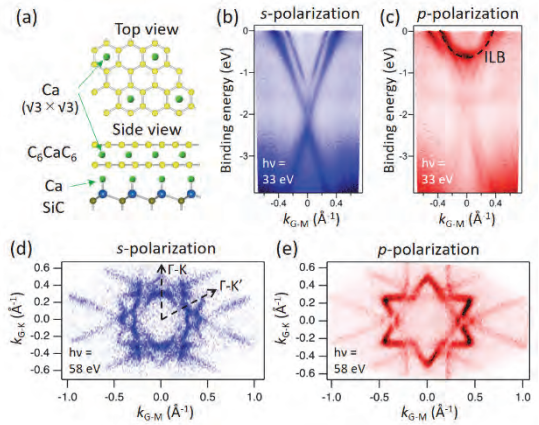


Fig. 1. (a) Schematic atomic model of Ca-intercalated bilayer graphene ($C_6CaC_6$) on Ca-terminated SiC substrate. (b)-(c) Band structure of $C_6CaC_6$ around Γ point, obtained by (b) *s*- and (c) *p*-polarized light. Parabolic band is stressed by the dashed guideline. (d), (e) Intensity mapping at Fermi level using (d) *s*- and (e) *p*-polarized light. Γ-K and Γ-K' direction are shown by dashed lines in (d). ARPES measurements were performed with hν = 33 or 58 eV under $T$ = 6 - 13 K.

[1] Y. Liu *et al.*, Phys. Rev. Lett. **107** (2011) 166803.
[2] C. Bao *et al.*, Phys. Rev. Lett. **126** (2021) 206804.
[3] T. E. Weller *et al.*, Nat. Phys. **1** (2005) 39.
[4] S. Ichinokura *et al.*, ACS Nano **10** (2016) 2761.
[5] H. Toyama *et al.*, ACS Nano **16** (2022) 3582.

BL3U

# Elucidation of the Function of Adsorbed Anions on the Surface of Cobalt Catalysts by Operando Observation

K. Harada[1], S. Tsunekawa[1], A. Sakai[1], M. Nagasaka[2] and M. Yoshida[1,3]
[1]*Yamaguchi University, Ube 755-8611, Japan*
[2]*Institute for Molecular Science, Okazaki 444-8585, Japan*
[3]*Blue Energy Center for SGE Technology (BEST), Ube 755-8611, Japan*

Recently, hydrogen production by electrolysis of water has been attracting attention. In this system, cobalt catalysts are known to be one of the efficient oxygen production catalysts [1]. Thus, various spectroscopic analyses have applied to the catalysts in order to investigate the physical properties and functions. However, the role of anions in the electrolyte solution is still not fully understood. From this background, in this study, the role of adsorbed anions on cobalt catalysts was investigated by attenuated total reflection infrared spectroscopy (ATR-IR) and X-ray absorption fine structure (XAFS) measurements under operando conditions.

The electrochemical cell was used with a Pt counter and an Ag/AgCl reference electrode. The cobalt catalyst was prepared by electrodeposition on Au thin film in a solution containing $Co^{2+}$ and carbonate anion (Co-$C_i$ catalyst). Under electrochemical control, the operando Co K-edge XAFS were measured by fluorescence mode in the PF BL-9A, and the operando O K-edge and C K-edge XAFS were measured by transmission mode at BL3U in the UVSOR synchrotron.

First, we checked the OER activity and found that Co-$C_i$ functioned as highly efficient water splitting catalyst. Next, SEM, EDX, and XPS measurements were also performed to confirm that the catalyst was electrodeposited on the substrate surface. Furthermore, the electrolyte solution was exchanged from potassium carbonate solution (K-$C_i$) to potassium sulfate solution (K-$S_i$) during monitoring the OER activity, indicating that the water splitting activity of the Co-$C_i$ catalyst was improved in the K-$C_i$ electrolyte solution.

To investigate the electronic state and local structure, the operando Co K-edge XAFS measurements were performed with the cobalt carbonate catalyst. EXAFS analysis showed that the peaks of Co-O and Co-Co bonds were observed at similar positions compared to the CoOOH reference sample, suggesting that the local structure of Co in the catalyst was consistent with that of CoOOH.

Then, operando O K-edge XAFS was measured, and the peak of Co(IV) as an active species [2-4] was observed at the electrode potential of water splitting reaction. This indicates the occurrence of high oxidation number Co in the Co-$C_i$ catalyst at the catalytic active potential.

Finally, the operando C K-edge XAFS measurements under the catalytic reaction (Fig. 1) showed that carbonate ions were adsorbed on the catalyst surface. The adsorbed peak was remained even after exchanging the electrolyte solution from K-$C_i$ to K-$S_i$. In addition, the same result was obtained in the operando ATR-IR measurement. Therefore, these results suggest that the carbonate ions are strongly adsorbed on the Co-$C_i$ catalyst to maintain the high oxidation number Co as active site.

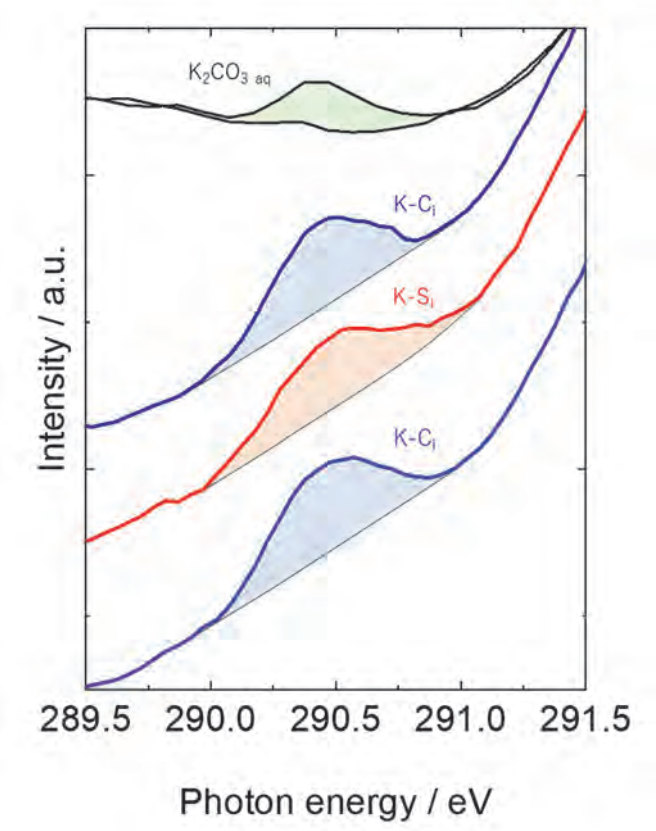


Fig. 1. Operando C-K edge XAFS spectra.

[1] W. Kanan, and D. G. Nocera, Science **321** (2008) 1072.
[2] A. M, Ullman, C. N. Brodsky, N. Li, S. L. Zheng, and D. G. Nocera, J. Am. Chem. Soc. **138** (2016) 4229.
[3] L. P. Wang, and T. Van Voorhis, J. Phys. Chem. Lett. **2** (2011) 2200.
[4] X. Li, and P. E. M. Siegbahn, J. Am. Chem. Soc. **135** (2013) 1380.

BL3B

# Evaluation of Interface Between Sapphire Substrate and UV Emitting Zinc Aluminate Phosphor Thin Films

H. Kominami[1], M. Endo[2], T. Kawashima[2], N. Sonoda[2], K. Inoue[2], N. Uesugi[2], K. Nie[2], A. Adachi[1], R. Ishihara[1], Y. Kamoi[1], A. Dorokhina[3] and S.Kurosawa[4,5]

[1]*Graduate School of Integrated Science and Technology, Shizuoka University, Hamamatsu 432-8651, Japan*
[2]*Faculty of Engineering, Shizuoka University, Hamamatsu 432-8651, Japan*
[3]*Graduate School of Science and Technology, Shizuoka University, Hamamatsu 432-8651, Japan*
[4]*New Industry Creation Hatchery Center (NICHe), Tohoku University, Sendai 980-8579, Japan*
[5]*Faculty of science, Yamagata University, Yamagata 990-8560, Japan*

The UV light is used for various applications depending on the wavelength as well as the sterilization described above. Recently, from the viewpoint of consideration to the environment, the mercury free UV emission devices have been demanded for the application of catalyst and medical situations. In our previous work, it was clarified that $ZnAl_2O_4$ phosphor was suitable for the UV field emission lamp because of its stability and luminescent property. It shows strong UV emission peaked around 250 nm which suitable for sterilization.

In this research, $ZnAl_2O_4$ thin film layer were prepared by thermal diffusion of ZnO and sapphire substrate for new UV devices. To obtain $ZnAl_2O_4$ thin film with high quality, we explore optimum condition of thermal annealing.

As a result of XRD of $ZnAl_2O_4$ annealed at 970 to 1050 °C, it was found that the peaks of (220), (311) and (333) appeared prominently, and polycrystalline $ZnAl_2O_4$ was formed. Figure 1 shows the full width of half maximum of diffraction peaks and these peak intensity ratio of each phase of $ZnAl_2O_4$ annealed at 970 to 1050 °C. Regarding the intensity ratio, the intensity ratio of each phase increased uniformly up to 990 °C, but at 1050 °C, the intensity ratio increased only in (333) and the intensity ratios of (220) and (311) decreased. From this result, it is considered that the growth is likely to occur in the orientation of (333) from a temperature exceeding a certain threshold value of 990 °C or higher.

Next, for $ZnAl_2O_4$ (333) that selectively grows on the c-plane sapphire substrate, the orientation of the c-plane sapphire substrate and the growth of $ZnAl_2O_4$ were investigated by evaluating the in-plane orientation by Φ scan measurement. Figure 2 shows a Φ scan of $ZnAl_2O_4$ (333) annealed at 970 to 1050 °C. Diffraction of (333) with the c-plane sapphire substrate was observed at 60° intervals. It is considered that both the c-plane sapphire substrate and (333) have the atomic arrangement of Aluminum atoms six-fold symmetric, and (333) has grown to inherit the six-fold symmetry of Aluminum of the c-plane sapphire substrate.

$ZnAl_2O_4$ was prepared at 970 to 1050 °C and evaluated by CL, XRD, SEM and the like. From the XRD results, it was found that the orientation of $ZnAl_2O_4$ (333) facilitates growth from temperatures above a certain threshold of 990 °C or higher. From the results of the Φ scan measurement, it is considered that (333) grows so as to inherit the six-fold symmetry of the atomic arrangement of Aluminum in the c-plane sapphire substrate.

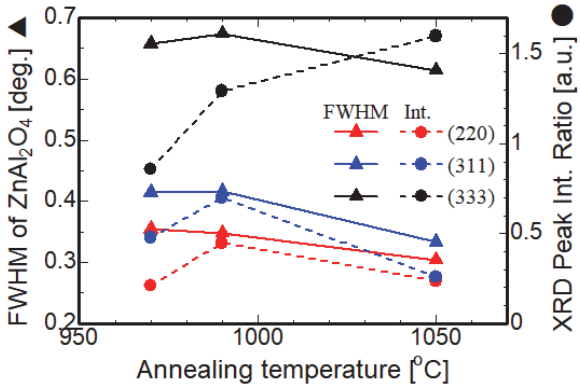


Fig. 1 ependence of FWHM and XRD Peak intensity of $ZnAl_2O_4$ thin films on annealing temperature.

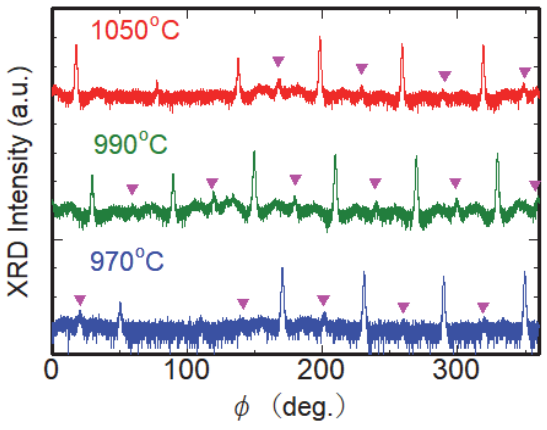


Fig. 2 Φ-scan of $ZnAl_2O_4$ (333) on c-plane sapphire substrate.

BL4U

# Application of Atomically-thin Graphene to X-ray Astronomy: Soft X-ray Transmission Measurements

I. Mitsuishi[1], K. Kashiwakura[1], Y. Niwa[1], T. Ogawa[1], M. Hirota[1], Y. Tawara[1], R. Kitaura[2], P. Solís-Fernández[3], K. Kawahara[3], H. Ago[3], T. Taniguchi[4], K. Nomoto[4], H. Kodaka[4], T. Ohigashi[5], H. Yuzawa[5] and K. Tanaka[5]

[1]*Graduate School of Science, Division of Particle and Astrophysical Science, Nagoya University, Nagoya 464-8602, Japan*
[2]*Department of Chemistry, Nagoya University, Nagoya 464-8602, Japan*
[3]*Global Innovation Center, Kyushu University, Kasuga 816-8580, Japan*
[4]*Optical Measurement Technology Development Department, R&D Division, USHIO INC., Yokohama 225-0004, Japan*
[5]*UVSOR Synchrotron Facility, Institute for Molecular Science, Okazaki 444-8585, Japan*

Thin films have been used in a variety of academic fields including astronomy. In X-ray astronomy, because X-rays are absorbed by the atmosphere of the Earth, balloons, rockets, and satellites are often used to observe X-rays from astronomical objects such as black holes, neutron stars, clusters of galaxies, and so on. Thin film devices have often been used in payloads of previous missions and playing a key role as, e.g., optical and contamination blocking filters and thermal shields [e.g., 1,2]. For such thin film devices, tolerance for severe launch and space environments and high transmission for more efficient use of limited observing time are required at the same time. Polyimide films have often been adopted because of relatively higher mechanical strength and heat tolerance in plastic materials. However, there is still room for improvement especially in transmission of a soft energy band below 1 keV. Thus, we have proposed to make use of graphene which is an atomically-thin material but has excellent mechanical and thermal properties at the same time. Our idea is to apply graphene to thin film devices in X-ray astronomy for the first time.

As a first step, we need to conduct X-ray transmission measurements to verify whether the transmission of graphene films especially in a soft energy band is actually high or not as expected because, as far as we know, no observed data is available except around 300 eV corresponding to the C K-edge structure. We prepared 5-layer free-standing graphene on a quartz substrate with a thickness of 200 μm with through holes with a diameter of 10 μm. To measure the number of X-ray photons with/without the 5-layer free-standing graphene collected by the Fresnel zone plate correctly, a taper structure with a taper angle of 30 degrees was prepared for each free-standing structure. The sample in the vacuum chamber and a close-up SEM image of the free-standing 5-layer graphene are shown in Fig. 1. Consequently, we obtained the transmission in 100, 140, 180, 220, 260, 340, 380, 420, 460, 500 eV, and the C K-edge structure between 280 and 320 eV in details successfully and confirmed that the observed transmission is very high as expected on the order of >89% corresponding to >97% for single-layer graphene although the transmission goes down to ~80 % in the C K-edge structure corresponding to ~95% for single-layer graphene as shown in Fig. 1 (Mitsuishi et al., in prep.). To investigate the impact of residual of the coated material, PMMA, on the free-standing graphene structure used in our fabrication process, we obtained transmission around the O K-edge structure even though the coated material was removed by using acetone. The observed transmission in 520—564 eV ranges from 95 to 98% and thus no strong contamination was found. To estimate the transmission more accurately, a systematic error such as a variation in the beam intensity should be taken into account in the near future.

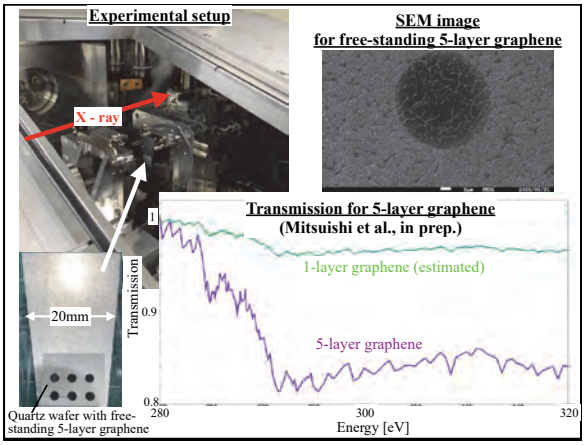


Fig. 1. Experimental setup with our sample and an example of the observed soft X-ray transmission curve.

[1] P.J. Serlemitos *et al.*, Publ. Astron. Soc. Japan **47** (1995) 105-114.
[2] P.J. Serlemitos *et al.*, Publ. Astron. Soc. Japan **59** (2007) S9-S21.

BL4B

# Annealing Effect on the Vacuum Ultraviolet Transmission Spectrum of Amorphous Selenium

K. Hayashi

*Department of Electrical, Electronic and Computer Engineering, Gifu University, Gifu 501-1193, Japan*

The decrease in the photoconductivity and the dark conductivity by long exposure to bandgap light have been observed in hydrogenated amorphous silicon [1] and amorphous chalcogenide materials [2]. This effect is usually called photodegradation and is explained in the creation of light-induced metastable defects (LIMD). Many models have been proposed for LIMD creation, but details of the mechanism for LIMD creation in these materials are still not clear. Recently, we have observed changes in photoconductivity in amorphous chalcogenide materials that cannot be explained by the creation of LIMD. The x-ray diffraction and the volume change of the films before and after irradiation of bandgap light suggest that the photoinduced phenomena is due to a change of the local structure of the amorphous network. Understanding the physical mechanism underlying metastability is one of the important fundamental problems related to these materials. In the previous reports, we reported the photoinduced effects on the vacuum ultraviolet (VUV) transmission spectrum of amorphous arsenic triselenide by the irradiation of the bandgap light. In this report, we study the annealing effect on the VUV transmission spectrum of amorphous selenium.

Sample used for the measurement of the VUV transmission spectra was amorphous Se (a-Se) thin film prepared onto thin aluminum film by conventional evaporation technique. The sample thickness was about 180nm. The aluminum film of the thickness of 200 nm was used to eliminate the higher order light from the monochromator in the VUV region. These measurements were carried out at room temperature on the BL4B beam line of UVSOR. The spectrum was measured by using the silicon photodiode as a detector. Two pinholes of 1.5mm in a diameter were inserted between the monochromator and sample to remove stray light. The intensity of the VUV light was monitored by measuring the TPEY of a gold mesh. The positions of the core levels for the samples were calibrated by referencing to the 2p core level absorption of the aluminum film.

Figure 1 shows annealing effect on the VUV transmission spectra of amorphous Se thin film. The VUV transmission spectrum of amorphous $As_2Se_3$ is also shown on the figure for reference. Annealing effect on the VUV transmission spectrum was investigated by annealing the amorphous Se with 353 K for 1 hour. Amorphous Se is thought to crystallize (polycrystalline) at this annealing temperature. As shown in the figure, each spectrum is very broad and multiple shoulders are observed. The absorption spectrum observed in the amorphous Se is roughly consistent with the previous report [3]. Main absorption peaks around 22nm corresponds to the 3d core level of Se atom. Although the wavelength resolutions in the spectral measurements are all the same, the spin-orbit splitting of the $3d_{5/2}$ and $3d_{3/2}$ level of Se atom is clearly resolved in amorphous $As_2Se_3$, while they are not clearly resolved in as-deposited amorphous Se and annealed amorphous Se. When amorphous Se crystallizes by annealing, it can be seen that the broad peak around 20 nm was composed of about three absorption peaks. It is not clear about the origin of broad spectra and several peaks. I think that these origins are related to the local structures of the amorphous network. The detailed experiments and analysis will be done in the next step. More detailed experiments are necessary to clarify the origin of the VUV transmission spectra.

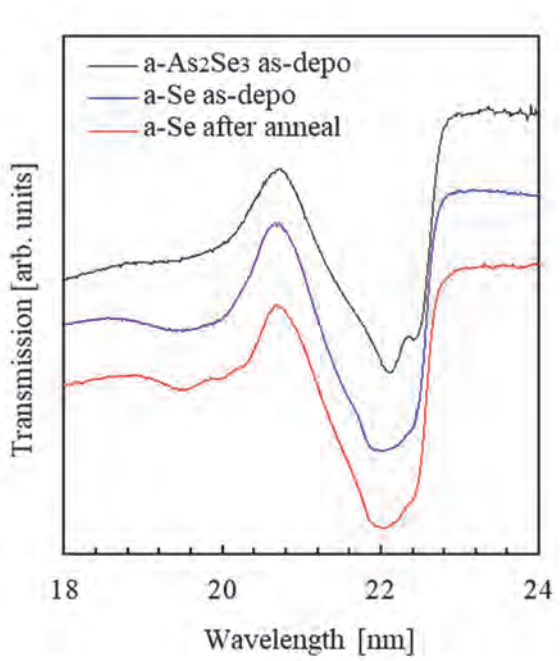


Fig. 1. Annealing effect on the VUV transmission spectra of a-Se thin film.

[1] D. L. Staebler and C. R. Wronski, Appl. Phys. Lett. **31** (1977) 292.
[2]K. Shimakawa, S. Inami, and S. R. Elliott, Phys. Rev. B **42** (1990) 11857.
[3] J. Bordas and J. B. West, Phil. Mag. **34** (1976) 501.

BL4B

# Magnetic Properties of CoPc/γ'-Fe4N Organic-inorganic Hybrid Interface

T. Miyamachi[1,2], H. Ono[1], Y. Umeda[1], K. Yamamoto[3,4], O. Ishiyama[3,4], T. Yokoyama[3,4] and M. Mizuguchi[1,2]

[1]*Department of Materials Science and Engineering, Nagoya University, Nagoya 464-8603, Japan.*
[2]*Institute of Materials and Systems for Sustainability (IMaSS), Nagoya University, Nagoya 464-8601, Japan.*
[3]*Institute for Molecular Science, Okazaki 444-8585, Japan*
[4]*The Graduate University for Advanced Studies (SOKENDAI), Okazaki 444-8585, Japan*

Organic materials are expected to be useful to spintronics devices due to their low spin current dissipation derived from weak spin-orbit interaction. In particular, an organic-inorganic hybrid interface has attracted much attention because its interface spin state can be controlled via the proximity effect. Spin-dependent electron transport properties of organic-inorganic hybrid system strongly depend on the domain size of organic molecular films, defect density and adsorption geometry of organic molecules. Thus, understanding structural, electronic and magnetic properties of the organic-inorganic interface on the level of single molecules is essential for realizing molecular spintronics devices. However, microscopic details of the hybrid interface have not been clarified so far.

In this study, we focus on fabricating organic-inorganic hybrid films with structurally controlled interface on the level of single molecules and investigating their intrinsic electronic and magnetic properties. For this purpose, ferromagnetic iron nitride atomic layers with γ'-$Fe_4N$ stoichiometry were chosen as an inorganic material, which uniformly grow and show high surface quality on the atomic scale [1,2]. Molecular layers composed of planer cobalt phthalocyanine (CoPc) were chosen as an organic material. Structural, electronic and magnetic properties of the hybrid interface composed of CoPc with the thickness of 1, 2 and 3 molecular layers and a bilayer γ'-$Fe_4N$ were investigated by scanning tunneling microscopy (STM), low energy electron diffraction (LEED) and x-ray absorption spectroscopy/magnetic circular dichroism (XAS/XMCD).

A bilayer γ'-$Fe_4N$ was prepared by iron deposition on Cu (001) with $N^+$ ion bombardment and subsequent annealing at 620 K. Then, CoPc/γ'-$Fe_4N$ hybrid thin films were fabricated by depositing CoPc on the γ'-$Fe_4N$ at room temperature. In combination with results of STM and LEED, the impact of the thickness of CoPc layers on the interfacial magnetic state was investigated by XAS/XMCD.

XAS/XMCD measurements were performed at BL4B in UVSOR by total electron yield mode at B = 0 - ± 5 T and T = 7.3 K. The XMCD spectra are obtained at the normal (NI: θ = 0°) and the grazing (GI: θ = 55°) geometries by detecting $\mu_+ - \mu_-$, where $\mu_+$ ($\mu_-$) denotes the XAS recorded at Fe and Co L adsorption edges with the photon helicity parallel (antiparallel) to the sample magnetization. Note that θ is the angle between the sample normal and the incident x-ray [3].

We find that the Fe orbital magnetic moment of the bilayer γ'-$Fe_4N$ evaluated by XMCD sum rule analysis changes with increasing thickness of the CoPc layer. The difference between the out-of-plane and in-plane Fe orbital magnetic moment, which is proportional to the magnetic anisotropy [4], is the largest when about one CoPc layer is deposited on the γ'-$Fe_4N$ and it decreases with further increasing thickness of the CoPc layer. The results suggest the perpendicular magnetic anisotropy of the γ'-$Fe_4N$ is enhanced by the magnetic coupling with CoPc molecules at the interface. STM and LEED observations reveal that the presence of the CoPc overlayers increases the surface roughness, which might in turn decrease the perpendicular magnetic anisotropy of the γ'-$Fe_4N$ arising from the formation of the CoPc/γ'-$Fe_4N$ hybrid interface through the intermolecular interaction between CoPc layers.

[1] Y. Takahashi *et al*., Phys. Rev. Lett. **116** (2016) 056802.
[2] Y. Takahashi *et al*., Phys. Rev. B **95** (2017) 224417.
[3] S. Nakashima *et al*., Adv. Funct. Mater. **29** (2019) 1804594.
[4] P. Bruno, Phys. Rev. B **39** (1989) 865.

BL4B

# Enhancement of the Perpendicular Magnetic Anisotropy in N-surfactant Assisted FeCo Ordered Alloy Thin Films

T. Miyamachi[1,2], Y. Umeda[1], H. Ono[1], K. Yamamoto[3,4], O. Ishiyama[3,4], T. Yokoyama[3,4] and M. Mizuguchi[1,2]

[1]*Department of Materials Science and Engineering, Nagoya University, Nagoya 464-8603, Japan.*
[2]*Institute of Materials and Systems for Sustainability (IMaSS), Nagoya University, Nagoya 464-8601, Japan.*
[3]*Institute for Molecular Science, Okazaki 444-8585, Japan*
[4]*The Graduate University for Advanced Studies (SOKENDAI), Okazaki 444-8585, Japan*

Skyrmions are nano-scale magnetic vortex structures, attracting great attention as a promising candidate of next-generation information storage devices due to their expected high magnetic stability and low critical current density for motion. Skyrmions can emerge in magnetic thin film hetero structures with the ferromagnetic/heavy metal interface. Since Dzyaloshinsky–Moriya interaction induced by 3d-5d hybridization effects is the driving force of the emergence of skyrmions in this system, the strict control of structural, electronic and magnetic properties of the interface in magnetic thin film hetero structures is quite important. Recently, we have revealed that large-area and atomically uniform iron nitride atomic layers with γ'-$Fe_4N$ stoichiometry can be grown on Cu(001) [1]. Thus, in this work, we intend to grow 5d heavy metal thin films on γ'-$Fe_4N$ atomic layers and fabricate the high quality 3d-5d heterointerface towards developing skyrmions-based novel magnetic structures. For this purpose, we first grow a monatomic layer of Co onto bilayer γ'-$Fe_4N$ and investigate the impact of the quality of 3d-3d heterointerface on electronic and magnetic properties of the system by low energy electron diffraction (LEED) and x-ray absorption spectroscopy/magnetic circular dichroism (XAS/XMCD).

To grow a bilayer γ'-$Fe_4N$, $N^+$ ion bombardment was first conducted with an incident energy of 500 eV onto Cu substrate and iron was additionally deposited at room temperature in ultra-high vacuum. The bilayer γ'-$Fe_4N$ was obtained by subsequent annealing at ~620 K. Appropriate growth conditions about the deposition amount of iron and annealing temperature were prechecked by atomically resolved surface characterizations using scanning tunneling microscopy (STM) [2]. Then, the low temperature deposition of a monatomic layer of Co at - 170 K was performed to fabricate Co-γ'-$Fe_4N$ magnetic thin film hetero structures. The sample was post-annealed at 300, 570 and 670 K and the annealing temperature dependence of electronic and magnetic properties was investigated by XAS/XMCD. XAS/XMCD measurements were performed at BL4B in UVSOR by total electron yield mode at B = 0 - ± 5 T and T = 7.9 K. The XMCD spectra are obtained at the normal (NI: θ = 0°) and the grazing (GI: θ = 55°) geometries. Note that θ is the angle between the sample normal and the incident x-ray. Element specific magnetization curves were also recorded by plotting the $L_3/L_2$ Fe and Co XAS intensities as a function of the magnetic field.

The XMCD signal of the bilayer γ'-$Fe_4N$ is greater in the GI geometry than NI geometry, which reveals its strong in-plane magnetic anisotropy as previously reported [1]. Adding one monolayer of Co activates the nitrogen surfactant effect [3,4], which leads to the formation of CoN in the topmost layer. Accordingly, we find from Fe magnetization curves that the out-of-plane magnetization of the Fe layer is relatively increased. The perpendicular magnetic anisotropy of the Fe layer is further enhanced by annealing at 570 K. However, at annealing temperature of 670 K, the decrease in the coercivity of the Fe layer is overserved. Taking the annealing temperature dependence of the LEED pattern into consideration, the enhancement of the out-of-plane magnetization could be caused by the improved ordering of the Co/Fe interface up to annealing temperatures of 570 K. At 670 K, surface N atoms start to desorb, which induces the interdiffusion of interfacial Co and Fe atoms and consequently lowers the coercivity.

[1] Y. Takahashi *et al*., Phys. Rev. B **95** (2017) 224417.
[2] Y. Takahashi *et al*., Phys. Rev. Lett. **116** (2016) 056802.
[3] K. Kawaguchi *et al*., Phys. Rev. Materials **4** (2020) 054403.
[4] K. Kawaguchi *et al*., Jpn. J. Appl. Phys. (accepted).

BL5U

# ARPES from Si{111} Facet Surfaces on Three-dimensional Lined Structures on Si(001) Substrates

K. Hattori[1], L. N. Pamasi[1], Y. Sakai[1], H. Yang[1], T. Shimizu[1], Y. Ida[3], W. Imayama[3], S. Tanaka[2], A. N. Hattori[2], S. Suga[2] and K. Tanaka[3]

[1]*Nara Institute of Science and Technology, Ikoma 630-0192, Japan*
[2]*SANKEN, Osaka University, Ibaraki, 567-0047, Japan*
[3]*UVSOR Synchrotron Facility, Institute for Molecular Science, Okazaki 444-8585, Japan*

Our information society has required highly densitized devices like 3D FET, which can break the restriction of miniaturizing 2D planar-type devices. To improve the specification (e.g., carrier mobility) of 3D devices, it is indispensable the control of 3D structure surfaces which are carrier passing region.

So far, our group have successfully created 3D Si surfaces by the combination of lithography and surface treatment techniques [1-7]: SEM, RHEED, LEED, or STM evaluations for lined or pyramidal structures with {111}, {110}, or {100} side/facet surfaces on (111), (110), or (001) substrates. In the beam time in 2021 FY, we focused electronic band investigations for 3D-Si surfaces, which promise side/facet-wall band engineering.

Figure 1 shows brief results for a 3D-Si lined structure (4 μm period) with {111} facet surfaces on a (001) substrate: (a) SEM image and (c) LEED pattern after the flash annealing in UHV. The LEED patterns clearly indicated 7×7 reconstruction on (111) and $(\bar{1}\bar{1}1)$ facet surfaces; the 7×7 spots move in right or left directions.

ARPES from the area including ≈13 $(\bar{1}\bar{1}1)$ facet-surfaces in geometry **A** (Fig. 1(d), note (111) is invisible) showed clear bulk-projected band dispersion and 7×7 surface bands: $S_1$-$S_3$, which guarantees well-controlled electronic states on the facet surfaces. ARPES from (111) mainly in geometry **B** ($\theta_e^c$ = 30° and $\theta_i$ = 27.5°) showed band dispersions at $\theta_e \lesssim$ 35.3° assigned from (111) and also dispersions below the (111) horizontal at $\theta_e \gtrsim$ 35.3° which could be assigned from glancingly radiated $(\bar{1}\bar{1}1)$ or the edge regions.

[1] A.N. Hattori, K. Hattori *et al*., Surf. Sci. **644** (2016) 86.
[2] A.N. Hattori, K. Hattori *et al*., Appl. Phys. Express **9** (2016) 085501.
[3]H. Yang, A.N. Hattori, K. Hattori *et al*., Jpn. J. Appl. Phys. **56** (2017) 111301.
[4] S. Takemoto, A.N. Hattori, K. Hattori *et al*., Jpn. J. Appl. Phys. **57** (2018) 090303.
[5] A.N. Hattori and K. Hattori, *21st Century Surface Science* (IntechOpen, London, 2020).
[6] A. Irmikimov, A.N. Hattori, K. Hattori, *et al*., ACS Cryst. Growth Des. **21** (2021) 946.
[7] S. Nakatsuka, T. Abukawa, A.N. Hattori, K. Hattori *et al*., e-J. Surf. Sci. NanoTechnol. **19** (2021) 13.

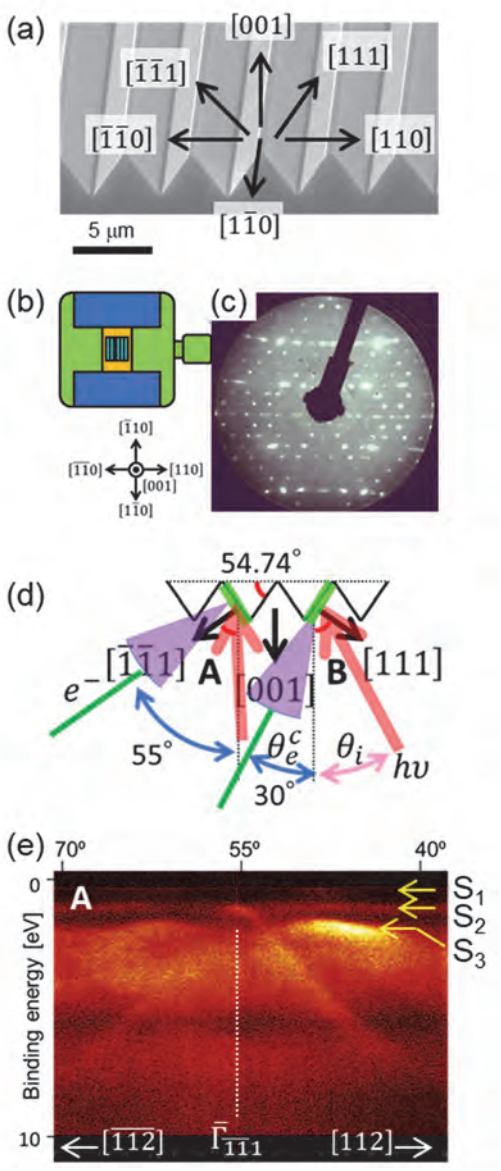


Fig. 1. (a) SEM image, (b) sample schematics on holder, (c) LEED pattern ($E_P$= 80 eV), (d) geometry of incident light (pink arrow) and electron emission (green line and fan-shaped purple) to sample, and (e) ARPES ($h\nu$= 60 eV, *p*-polarization; $\phi$= 50 μm, acceptance angle≈ ±15°, light-analyzer angle= 57.5°) in geometry **A** at $\theta_e^c$ = 55° ($\theta_i$ = 2.5°), for 3D facet-lined structures with Si{111} facet surfaces on Si(001) substrates.

BL5U

# Electronic Structure of K Adsorbed SmS Surface

T. Nakamura[1,2], T. Nakaya[2], H. Sugihara[2], K. Tanaka[3], K. Imura[4], H. S. Suzuki[5], N. K. Sato[4] and S. Kimura[1,2,3]

[1]*Graduate School of Frontier Biosciences, Osaka University, Suita 565-0871, Japan*
[2]*Department of Physics, Graduate School of Science, Osaka University, Toyonaka 560-0043, Japan*
[3]*Institute for Molecular Science, Okazaki 444-8585, Japan*
[4]*Department of Physics, Graduate School of Science, Nagoya University, Nagoya 464-8602, Japan*
[5]*Institute for Solid State Physics, The University of Tokyo, Kashiwa 277-8581, Japan*

Samarium mono-sulfide (SmS) is a typical valence fluctuation material [1]. At ambient pressure, SmS is a semiconductor with an indirect bandgap of about 0.1 eV, and its color is black [2]. The electrical properties change to metallic above a critical pressure of 0.65 GPa. Although the pressure-induced phase transition was discovered over 50 years ago [1], the origin of the phase transition is still under debate. Recently, a phase transition like the pressure-induced one has been reported due to two different types of perturbations: light irradiation and current injection [3,4]. These perturbations are commonly expected to increase carriers, but the detailed electronic states after carrier doping have not been clarified yet.

Alkali metal adsorption on crystal surfaces is widely used as a typical method to investigate the effect of carrier injection into a material. Due to the charge transfer of the free-electron-like outermost electrons in the alkali metal to SmS, a carrier-doped SmS surface can be realized. In this work, we have studied the change of the electronic structure by potassium (K) doping on a SmS surface by synchrotron-based ARPES.

A high-quality single-crystalline SmS was grown by the vertical Bridgman method in a high-frequency induction furnace. The clean SmS surface was obtained by cleaving in-situ in an ultra-high vacuum chamber. K atoms were evaporated from the well-degassed alkali metal dispenser (SAES-Getters) at room temperature (RT).

Figure 1(a) shows the ARPES intensity plot of the pristine-SmS along the $\bar{\Gamma}$ - $\bar{X}$ line of the surface Brillouin zone taken with 60-eV photons. Flat $Sm^{2+}$ $4f^5$ multiplet structure and dispersive S 3*p* bands were observed. After the K deposition as shown in Fig. 1(b), the band dispersion of the Sm 4*f* states was changed without a higher binding energy shift due to the natural electron doping. These results suggest that the K adsorption on SmS caused a deformation of the band structure, which cannot be explained as a simple rigid band shift model due to electron doping.

[1] A. Jayaraman *et al.,* Phys. Rev. Lett. **25** (1970) 1430.
[2] K. Matsubayashi *et al.,* J. Phys. Soc. Jpn. **76** (2007) 064601.
[3] R. Kitagawa *et al*., Appl. Phys. Lett. **82** (2003) 3641.
[4] H. Ando *et al*., JPS Conf. Proc. **30** (2020) 011132.

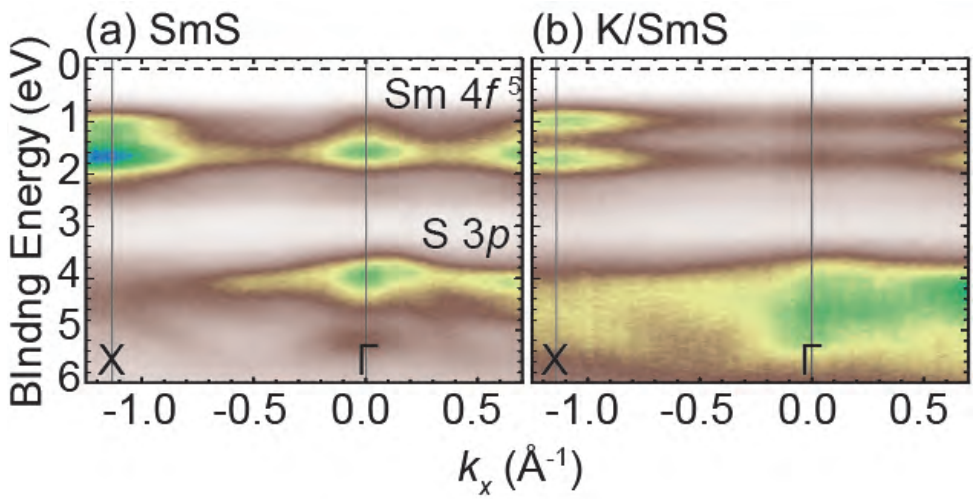


Fig. 1. ARPES intensity plots of (a) pristine SmS and (b) K-adsorbed SmS along $\bar{\Gamma}$-$\bar{X}$ with 60-eV photons at room temperature.

BL5U

# Explorations for Spontaneously Formed Excitons in Narrow-gap Semiconductors and Semimetals

K. Fukutani[1,2], M. Murakami[3], C.I. Kwon[4,5], J. S. Kim[4,5], K. Tanaka[1,2], S. Kera[1,2,3]
[1]*Institute for Molecular Science, Okazaki 444-8585, Japan*
[2]*The Graduate University for Advanced Studies (SOKENDAI), Okazaki 444-8585, Japan*
[3]*Graduate School of Science and Engineering, Chiba University, Chiba 263-8522, Japan*
[4]*Center for Artificial Low-Dimensional Electronic Systems, Institute for Basic Science, Pohang, Korea*
[5]*Pohang University of Science and Technology, Pohang, Korea*

Excitons are bound pair of an electron and a hole, conventionally produced transiently by irradiation of light on semiconductors, and is one of the most fundamental quasiparticles in solids and molecular materials that play central roles in various quantum devices, such as photovoltaic cells, light emitting diodes and photodetectors.

In recent years, a new exotic phase of matter called an excitonic insulator has garnered much attentions. In the excitonic insulator phase, at sufficiently low temperature, the electrons and holes are spontaneously bound to form an excitons and undergo quantum condensation.

Among the various candidate materials for excitonic insulator, $Ta_2NiSe_5$ is particularly suitable for the experimental investigations as it exhibits a direct band gap and the excitonic insulator transition accompanies only a minor structural distortion, which preserves the periodicity of the material. For this relative simplicity, $Ta_2NiSe_5$ has been investigated extensively in the past decade by various experimental methods [1] and it is widely conceived to be a Bose-Einstein condensation (BEC)-type excitonic insulator.

Of particular interest in the BEC-type excitonic insulator is the theoretical prediction of the intermediate phase called "preformed exciton phase", which is believed to appear between the excitonic insulator and the normal phases (see Fig. 1) [2]. In the preformed exciton phase, the magnitude of the bandgap is small enough (i.e., the free carrier screening is small enough) to allow for the bound state for the electrons and holes, yet the temperature is too high for these spontaneously formed excitons to undergo the Bose-Einstein condensation. Therefore, this particular region of the phase diagram supports the existence of finite number of excitons in equilibrium. In our recent study [3], the direct photoemission signal from these spontaneously formed excitons have been detected and long-standing theoretical prediction has been confirmed. However, the detailed formation mechanism of such excitons is still elusive due to the lack of experimental data for this particular phase of excitonic insulator materials.

Thus, in order to pin down the origin of these spontaneously formed excitons, we are performing a series of angle-resolved photoemission spectroscopy (ARPES) experiments at BL5U for the chalcogen-substituted compounds $Ta_2Ni(Se_{1-x}S_x)_5$ for various compositions $x$. In the experiments, the freshly cleaved samples of $Ta_2Ni(Se_{1-x}S_x)_5$ have been measured to reveal their band structures as well as to explore for the photoemission signals from the spontaneously formed excitons as a function of temperature, photon energy as well as the light polarizations.

A representative result of the ARPES intensity plot is shown in Fig. 2. It can be seen that the photoemission signal from excitons, observed in $Ta_2NiSe_5$ [3] is also observed for the S-substituted compounds.

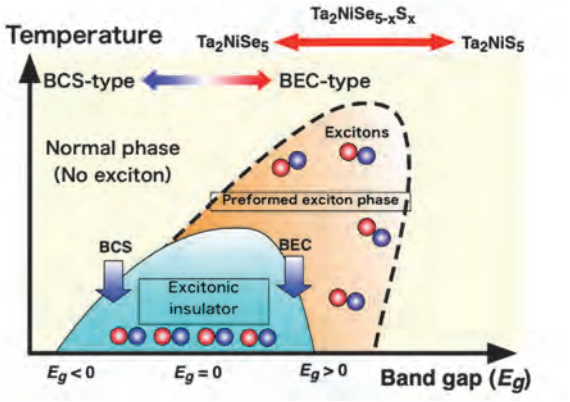


Fig. 1. Theoretical phase diagram of excitonic insulators.

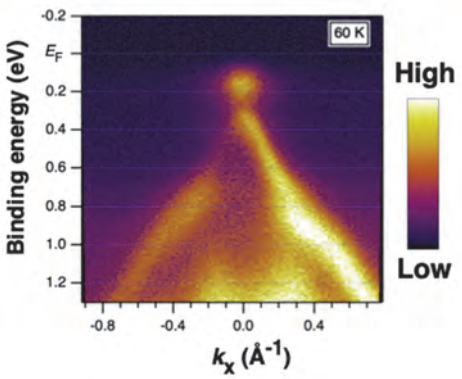


Fig. 2. ARPES intensity plot for chalcogen-substituted excitonic insulator $Ta_2Ni(Se_{1-x}S_x)_5$.

[1] Y. Wakisaka *et al.*, Phys. Rev. Lett. **102** (2009) 026402; Y.F. Lu *et al.*, Nat. Commun. **8** (2017) 14408.
[2] F.X. Bronold *et al.*, Phys. Rev. B **74** (2006) 165107.
[3] K. Fukutani *et al.*, Nat. Phys. **17** (2021) 1024.

BL5B

# X-ray Absorption Spectroscopy Measurements of Au/Fe/MgO Sandwich Structure Sample for Study of Soft X-ray Second Harmonic Generation

T. Sumi[1], M. Horio[1], X. Zhang[1], T. Kato[2] and I. Matsuda[1,3]

[1]*Institute for Solid State Physics, The University of Tokyo, Kashiwa 277-8581, Japan*

[2]*Institute of Materials and Systems for Sustainability, Nagoya University, Nagoya 464-8603, Japan*

[3]*Trans-scale Quantum Science Institute, The University of Tokyo, Tokyo 113-0033, Japan*

Second harmonic generation (SHG), which is a phenomenon that occurs by the interaction between light and a system where the inversion symmetry is broken, has been used not only to convert light to higher frequencies but also to investigate electronic states of molecules at the systems in the visible region. After the construction of X-ray Free Electron Laser (XFEL) such as Pring-8 Angstrom Compact free-electron LAser (SACLA), we have been developing SHG methods in the range of soft X ray, and applied to $GaFeO_3$ [1], $LiNbO_3$ [2], $LiOsO_3$ [3], and GaAs [4]. By setting the incident energy to the inner-shell core level, SHG acquires element selectivity by inner-core excitation resonance. Although this technique is useful to reveal the electronic states of the targeted atoms at surfaces/interfaces, there is no report for the interface SHG.

In this research, at UVSOR BL5B, we conducted X-ray absorption spectroscopy for a Fe film sandwiched by films of Au and MgO to grasp the possibility of the occurrence of soft X-ray SHG before observing it. We synthesized the sample by ultrahigh vacuum molecular beam epitaxy method. The sandwich structure of Au/Fe/MgO was repeated 4 times. The structure of the sample is [Au (2 nm)/Fe (2 nm)/MgO (2 nm)]$_4$/MgO(001, substrate) (Fig. 1). The sample was placed perpendicular to the incident beam, and the drain current was measured.

Figure 2 shows a XAS spectrum around the Fe *M*-edge. The drain current, I, was normalized by incident intensity, $I_0$, measured by the Au mesh. The result shows Fe *M*-edge (53 eV) absorption peak appears. This means that the Fe *M*-edge dipole transition is allowed. To investigate the transition around the SHG energy (106 eV), the drain current was measured around that energy without the Au mesh to prevent the effect of the mesh (Fig. 3). The peak appears around 106 eV. These results suggest that the dipole transitions in the SHG process starting from Fe *M*-shell are allowed.

In conclusion, we investigated the electric dipole transition for the Au/Fe/MgO sandwich structure sample by XAS and found the possibility of the SHG process starting from the Fe *M* shell ($h\nu$ = 53 eV). It is expected that SHG originating from the interfaces is available. Furthermore, it is possible to achieve soft X-ray magnetization-induced SHG (MSHG) by applying a magnetic field to this sample because it has perpendicular magnetization anisotropy (PMA).

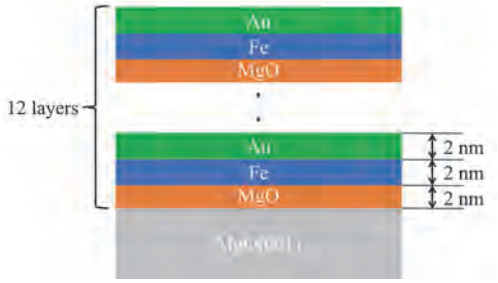


Fig. 1. Structure of the [Au/Fe/MgO]$_4$ / MgO(001) sandwich structure sample.

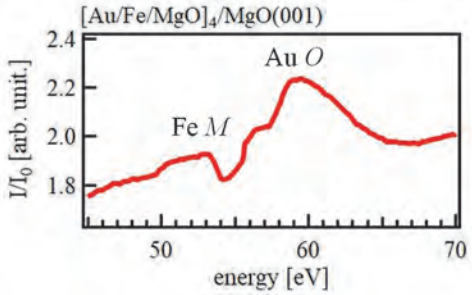


Fig. 2. XAS spectrum for the sandwich structure sample around Fe *M*-edge.

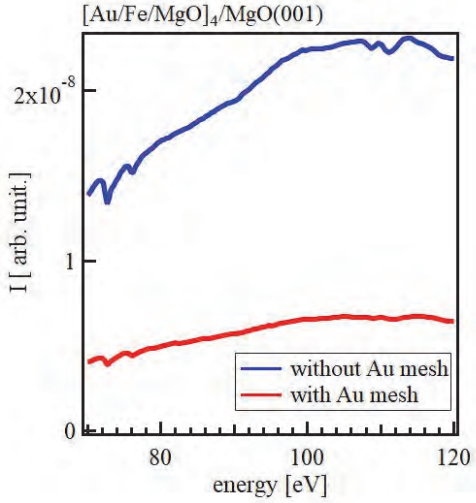


Fig. 3. Drain current of the sandwich structure sample without (blue) and with (red) the Au mesh.

[1] Sh. Yamamoto *et al.*, Phys. Rev. Lett. **120** (2018) 223902.
[2] E. Berger *et al.*, Nano Lett. **21** (2021) 6095.
[3] C. B. Uzundal *et al.*, Phys. Rev. Lett. **127** (2021) 237402.
[4] T. Sumi *et al.*, e-J. Surf. Sci. Nanotech. (2022) (accepted).

BL6U

# Bromine Doping to Perylene Monolayer on Au(110): Photoelectron Momentum Microscopy

O. Endo[1,3], F, Matsui[2], S. Kera[2], W. -J. Chun[3], M. Nakamura[4], K. Amemiya[5] and H. Ozaki[1]

[1]*Department of Organic and Polymer Materials Chemistry, Faculty of Engineering, Tokyo University of Agriculture and Technology, Koganei 184-8588, Japan*

[2]*UVSOR Synchrotron Facility, Institute for Molecular Science, Okazaki 444-8585, Japan*

[3]*Graduate School of Arts and Sciences, International Christian University, Mitaka 181-8585, Japan*

[4]*Department of Applied Chemistry and Biotechnology, Faculty of Engineering, Chiba University, Chiba 263-8522, Japan*

[5]*Photon Factory, High Energy Accelerator Research Organization (KEK-PF), Institute of Materials Structure Science (IMSS), Tsukuba 305-0801, Japan*

Energy level alignment at organic-metal interface is one of the important topics in the field of organic electronics [1]. The HOMO and LUMO levels of organic molecules shift upon adsorption as a result of the work function change due to the formation of an interfacial dipole. This causes the change of the charge injection barrier from the metal electrode, which affects the efficiency of the organic devices. Recently, doping of organic semiconductors is re-focused to improve the conductivity [2]. The doping process in organic semiconductors is the charge transfer between the molecules, and two representative mechanisms are proposed: one is the integer charge transfer, or ionization, and the other is the formation of charge transfer complex [2]. In either case, the energy levels of the doped molecule are altered from those of the original HOMO or LUMO, because of the electrostatic effect derived from the doped charge, or the orbital re-hybridization. Therefore, the energy level alignment of the doped molecules at the metal interface is necessary to be elucidated. In this study, we have observed the electronic structure of perylene molecules on the Au(110) surface and the effect of bromine doping by angle resolved photoelectron spectroscopy (ARPES) and X-ray photoelectron spectroscopy (XPS) using momentum microscope, which has recently been introduced at BL6U.

Figure 1(a) shows the ARPES results of the perylene monolayer on the Au(110)-(1x2) surface, which was obtained at $E_b$ = 1.5 eV at the surface normal direction. The photoelectron pattern simulated for the HOMO of the perylene molecule at the normal direction with respect to the molecular plane is shown in Fig. 1(c), right panel, which was obtained by the plane wave approximation. This four-fold pattern is changed to a two-fold one for the ±18° off-nomral direction, as shown in Fig. 1(b). The pattern resemblance for Fig. 1(a) and 1(b) indicates that the molecular plane is tilted ±18° with respect to the surface normal. The tilted molecular orientation is in accordance with the results of X-ray absorption spectroscopy (XAS), and the scanning tunneling microscopy [3]. Figure 1(d) depicts the structural model of perylene on Au(110)-(1x2).

Bromine molecules doped to the perylene monolayer penetrate into the monolayer and adsorbed dissociatively on the Au(110) surface. This was confirmed by the Br-3d XPS spectra. Upon bromine penetration, the orientation of the perylene molecules become random. Therefore, the characteristic ARPES pattern of the HOMO electrons disappears. The XAS results indicates that the perylene molecules are cationized upon bromine doping, because of the charge transfer from the perylene to the Au surface mediated by the bromine layer. The HOMO level exceeds the Fermi level as a result of the upward energy shift of the perylene MOs induced by the bromine layer, and hence, part of the HOMO electron is transferred. The energy shift was confirmed by the C-1s XPS spectra.

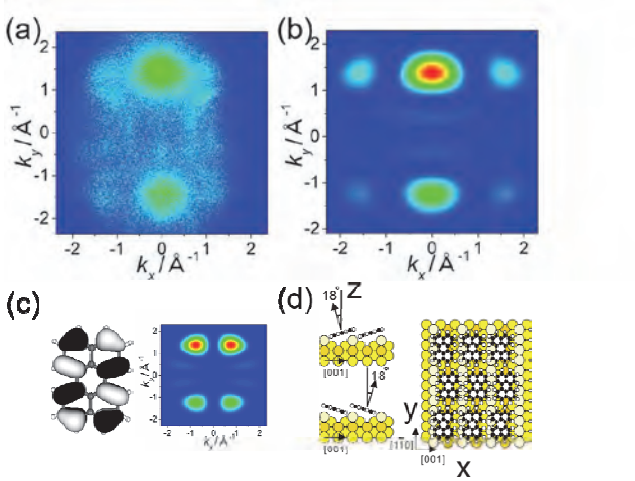


Fig. 1. (a) Momentum map of perylene/Au(110) at $E_b$ = 1.5 eV. (b) Simulated photoelectron distribution for perylene molecule tilted ±18° along the short axis. (c) Orbital distribution of perylene HOMO and the simulated photoelectron distribution at the normal direction with respect to the molecular plane. (d) Structural model of perylene on Au(110).

[1] H. Ishii, *et al.,* Adv. Mater. **11** (1999) 605.
[2] I. Salzmann, *et al.,* J Electron Spectros Relat Phenomena **204** (2015) 208.
[3] L. Gross, *et al.,* Org. Electron. **3** (2002) 1.

BL6U

# High-resolution Photoelectron Momentum Microscope Study on the Electronic Structure of Charge-density-wave Material

K. Fukutani[1,2], S. Tanaka[3], F. Matsui[1,2] and S. Kera[1,2,4]
[1]*Institute for Molecular Science, Okazaki 444-8585, Japan*
[2]*The Graduate University for Advanced Studies (SOKENDAI), Okazaki 444-8585, Japan*
[3]*Sanken, Osaka University, Ibaraki 567-0047, Japan.*
[4]*Graduate School of Science and Engineering, Chiba University, Chiba 263-8522, Japan*

Among various critical phenomena in solids, charge density wave (CDW) is one of the widely observed phase transitions, which induces deformation of lattice periodicity as well as of the electronic density. The prototypical examples of such CDW are found in many of the transition metal dichalcogenides (TMDCs), which exhibit the wide range of periodicities upon the phase transitions, including commensurate and incommensurate CDWs [1].

On the other hand, despite the ubiquity of CDWs and the decades-long intensive research efforts, aimed for revealing their microscopic mechanisms, there is no clear consensus on their driving forces.

Recently, the roles of dimensionalities on the properties of TMDC materials and their CDWs have attracted much attentions. In particular, in the two-dimensional limit (i.e., a single monolayer), some TMDC materials are found to behave in drastically different manners, as can be seen in two-dimensional ferromagnetism of $VSe_2$ [2], the suppression of CDW in $TaS_2$ [3], and the enhancement of CDW in $NbSe_2$ [4], to name a few. These recent observations show that the careful studies of the dimensionality effects can provide key insights in resolving the long-standing mysteries of the origin of CDW transitions.

Among such TMDC materials, the series of titanium dichalcogenides, $TiX_2$ (X = S, Se, Te) present particularly interesting trends in CDW properties. While in the bulk form, only $TiSe_2$ exhibits CDW, in the two-dimensional limit, CDW with the same periodicity emerges for $TiTe_2$ [5], suggesting the role of dimensionality in the emergence of CDW.

However, it has been reported that the choice of substrate affects significantly the CDW order [6]. This is most naturally attributed to the interactions between the monolayer $TiTe_2$ and the substrate. In other words, while the dimensionality is a critical factor for CDW formation, the degree to which the monolayer-substrate interaction breaks the "pure" two-dimensionality of $TiTe_2$ is a critical issue that must be systematically investigated.

In this project, we attempt to tune the dimensionality quasi-continuously by inserting the intercalation layer with various atomic thicknesses near the surface of bulk $TiTe_2$, whereby gradually "lifting up" the two-dimensional layer to investigate the respective electronic structures.

For this purpose, photoelectron momentum microscope (PMM) is an ideal instrument, which can efficiently identify the periodicity and the topology of the Fermi surface structure in wide momentum range. In the first phase of this project, we have performed the high-resolution PMM measurements on pristine $TiTe_2$.

Combined with the use of space-resolved mode, the surface of high crystallinity can be readily found and the example of the obtained spectra is shown in Fig. 1. The experiments were performed with photon energy as well as polarization dependence, and the obtained set of data are expected to yield detailed information on the three-dimensional ($k_x$, $k_y$, $k_z$) electronic structures as well as their orbital textures.

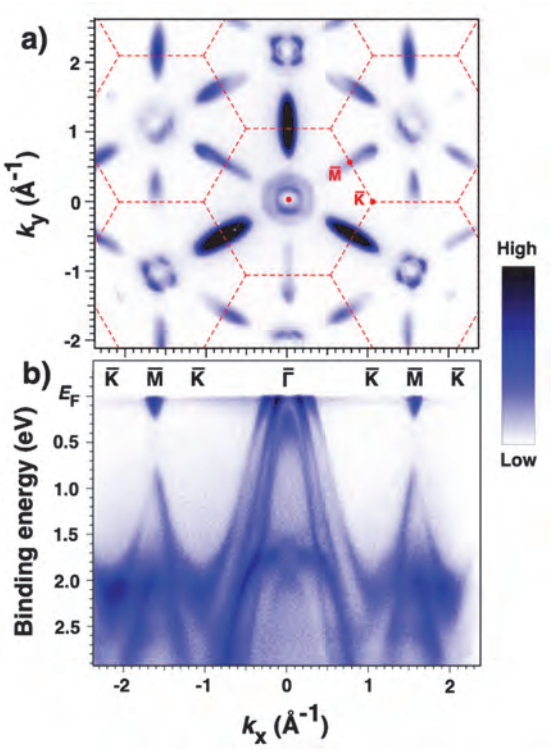


Fig. 1. (a) Fermi surface intensity image and (b) band structure mapping of $TiTe_2$ obtained at $h\nu$ = 52 eV and $T$ = 50 K with PMM at BL6U.

[1] K. Rossnagel, J. Phys.: Condens. Matter **23** (2011) 213001.
[2] M. Bonilla *et al.*, Nat. Nanotechnol. **13** (2018) 289.
[3]C. E. Sanders *et al.*, Phys. Rev. B **94** (2016) 081404(R).
[4] X. Xi *et al.*, Nat. Nanotechnol. **10** (2015) 765.
[5] P. Chen *et al.*, Nat. Commun. **8** (2017) 516.
[6] M.-K. Lin *et al.*, Phys. Rev. Lett. **125** (2020) 176405.

BL6U

# Twin-domain Boundary and Monoatomic Step of Graphite Surface Imaged by Photoelectron Momentum Microscopy

F. Matsui[1,2], Y. Okano[1], H. Matsuda[1], T. Yano[1], E. Nakamura[1], S. Kera[1,2] and S. Suga[3,4]

[1]*UVSOR Synchrotron Facility, Institute for Molecular Science, Okazaki 444-8585, Japan*

[2]*The Graduate University for Advanced Studies (SOKENDAI), Okazaki 444-8585, Japan*

[3]*SANKEN, Osaka University, Suita, Osaka 567-0047, Japan*

[4]*Forschungszentrum Jülich, Germany*

The photoelectron momentum microscope is an instrument that combines a photoelectron microscope with a projection-type electron energy analyzer to enable both μm-scale valence band mapping and momentum-selective photoelectron microscopy [1-3]. Using these methods, we measured the local electronic structure of graphite crystal surfaces.

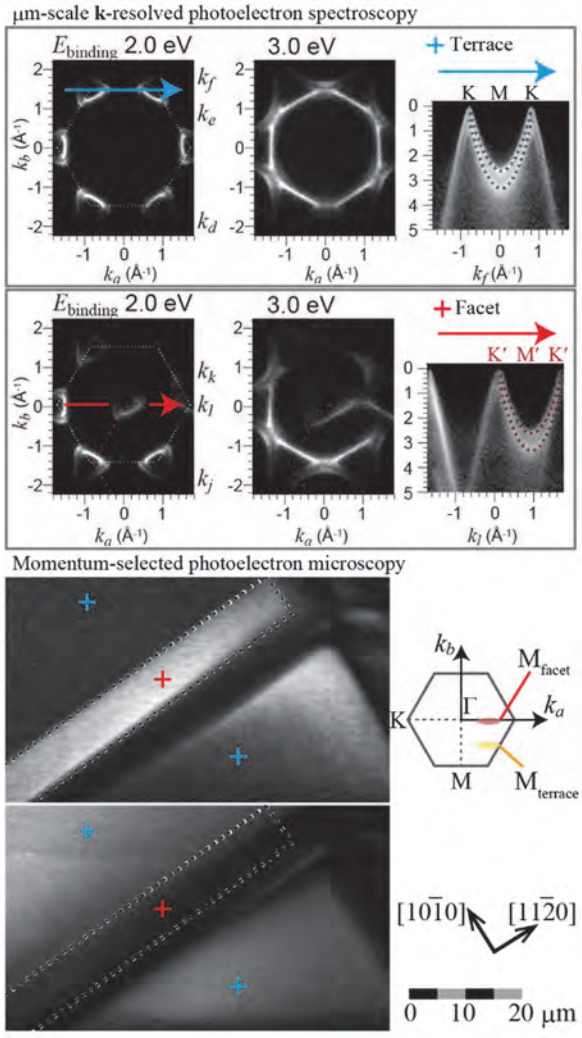


Fig. 1. μm-scale valence band mapping and momentum selective photoelectron microscopy of graphite surface.

The cleaved graphite surface is found to have facets a few μm wide that share a twin-domain boundary in the armchair edge direction. This "armchair facet" was characterized by μm-scale VB mapping. The normal direction of the "armchair facet" differed from that of the terrace region by about 20°. The π-band splitting due to interlayer interaction was the same in the "armchair facet" and the terrace region, indicating that the interlayer distance between the two regions was identical. By transforming the photoelectron distribution of the selected momentum direction in reciprocal space to real space, a momentum-selective microscopic image can be obtained. By detecting photoelectrons of the "armchair facet" at the M symmetry point, a microscopic image in which the "armchair facet" is selectively enhanced was successfully obtained [4].

Furthermore, the $k_z$ dispersion of graphite from the few mm region was measured using photoelectron momentum microscope (Fig. 1). The π band dispersion over the entire Brillouin zone was investigated. Note that graphite crystals with an *ABAB*…-type stacking structure are six-fold symmetric around the *z* axis, whereas a surface with one type of termination is three-fold symmetric. The microscope function of the PMM has a detection area sufficiently small to select only one type of graphite termination structure on the cleavage plane. We found that the π band was no longer degenerate in the ALH plane and its symmetry was reduced from $C_{6v}$ to $C_{3v}$. This phenomenon is attributed to the coupling of the single-domain three-fold graphite surface π-band with the six-fold bulk $k_z$ dispersion, which has been neglected up to now. This symmetry breaking was used to image the monatomic steps on the graphite surface [5].

[1] F. Matsui S. Makita, H. Matsuda, T. Yano, E. Nakamura, K. Tanaka, S. Suga, and S. Kera, Jpn. J. Appl. Phys. **59** (2020) 067001.

[2] S. Makita, H. Matsuda, Y. Okano, T. Yano, E. Nakamura, Y. Hasegawa, S. Kera, S. Suga, and F. Matsui, e-J. Surf. Sci. Nanotech. **19** (2021) 42.

[3] F. Matsui, S. Makita, H. Matsuda, E. Nakamura, Y. Okano, T. Yano, S. Kera, and S. Suga, J. Phys. Soc. Jpn. **90** (2021) 124710.

[4] F. Matui, Y. Okano, H. Matsuda, T. Yano, E. Nakamura, S. Kera, and S. Suga, submitted (2022). "Domain-resolved Photoelectron Microscopy and μm-scale Momentum-resolved Photoelectron Spectroscopy of Graphite Armchair Edge Facet".

[5] F. Matui and S. Suga, submitted (2022) "Coupling of graphite surface π band with $k_z$ dispersion"

BL6U

# Development of the Fabrication System for the μm-scale Ultra-thin Film at BL6U

T. Nakamura[1,2], F. Matsui[3] and S. Kimura[1,2,4]

[1]*Graduate School of Frontier Biosciences, Osaka University, Suita 565-0871, Japan*
[2]*Department of Physics, Graduate School of Science, Osaka University, Toyonaka 560-0043, Japan*
[3]*UVSOR Synchrotron Facility, Institute for Molecular Science, Okazaki 444-8585, Japan*
[4]*Institute for Molecular Science, Okazaki 444-8585, Japan*

Photoelectron spectroscopy (PES) is a powerful technique to investigate the electronic structures of materials. Recently developed at UVSOR-III BL6U, synchrotron-based photoelectron momentum microscopy (PMM) is one of the state-of-the-art PES systems [1]. On the other hand, research on unique electronic states in the microscopic region, such as edge states in topological materials and domains in inhomogeneous samples, has been intensively explored [2-4]. The combination of PMM and small-sized samples with the unique electronic state leads to fertile physics. In this work, we have developed a new thin-film deposition system in the preparation chamber at the BL6U end station.

The basic concept of this system is the selective deposition of the materials passes through the spatial mask filter from the evaporator. Figure 1(a) shows the photo of the flagship-type sample holder with two M2 holes to attach the additional filter component. Spot-welded Ta foils are used to fix a substrate. Figure 1(b) shows the mask filter. The main material is a flat Ta foil (10 × 10 $mm^2$) with a φ2 mm hole at the center. A honeycomb-type TEM grid (The hole and bar sizes on the TEM grid are 290 μm and 59 μm, respectively) was used to make a pattern in the current system. A commercially available square clip (4 × 4 $mm^2$) is used as a handle to fix the mask on the sample. The opposite side of the clip is an M2 screw. Figure 1(c) shows the photo of the sample holder with the mask filter on a heating stage in the preparation chamber of the BL6U end station. The distance between the holder and mask filter is about 1.5 mm. When cleaning the substrate by annealing and Ar sputtering, the mask filter is removed and set to other sample holders on the sample bank.

We used the InSb(111)B substrate as a test sample. The substrate was cleaned by the cycle of Ar-ion sputtering (acceleration energy of 1 kV) and annealing up to 600 K. After checking the sharp (3 × 3) diffraction pattern, the 1-nm Sb layer was evaporated on the InSn(111)B substrate with the mask filter at room temperature.

Figure 2 shows a spatial-resolved In 4*d* core level intensity map. One pixel indicates the sum of the photoelectron intensity measured by the microscopy mode of PMM. The domain scale of the bright area is almost consistent with the size of the bar of the TEM grid.

As the next step, we quantitively evaluate the spatial resolution of selective deposition with mask filters and observe the band structure from a single micro-scale domain.

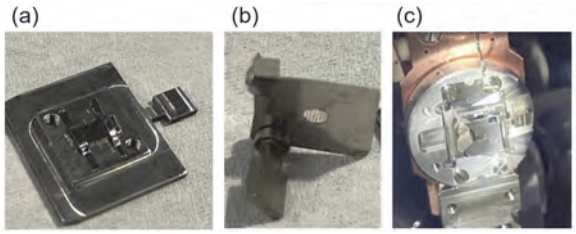


Fig. 1. Photos of the spatially selective deposition system. (a) sample holder. (b) mask filter. (c) sample holder with mask filter on a heating stage in the preparation chamber of BL6U.

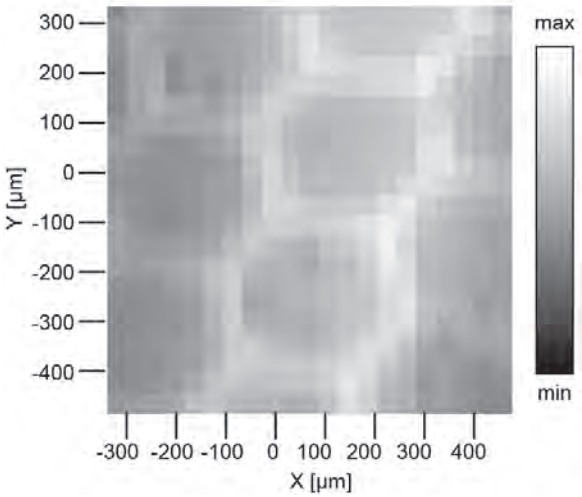


Fig. 2. Real-space image of the In 4*d* photoelectron intensity plot. The incident photon energy is 80 eV.

[1] F. Matsui *et al.,* Jpn. J.Appl. Phys. **59** (2020) 067001.
[2] K. Nakayama *et al*., Nano Lett. **19** (2019) 3737.
[3] R. Noguchi *et al*., Nature **566** (2019) 518.
[4] H. Iwasawa, Electron. Struct. **2** (2020) 043001.

BL7U

# High-resolution Angle-resolved Photoemission Study on $MnBi_2Se_4/Bi_2Se_3/MnBi_2Se_4$ Sandwich Structure

R. Fukushima[1], S. Ichinokura[1], K. Tanaka[2] and T. Hirahara[1]
[1]*Department of Physics, Tokyo Institute of Technology, Tokyo 152-8551, Japan*
[2]*UVSOR Synchrotron Facility, Institute for Molecular Science, Okazaki 444-8585, Japan*

Topological insulators (TI) are extensively studied recently due to its peculiar properties [1]. The Dirac-cone surface states of TI are protected by time-reversal symmetry (TRS) and backscattering among these surface states is prohibited. But when TRS is broken by application of a magnetic field or incorporating magnetic materials, a gap opening in the Dirac cone is expected and an intriguing phase called the quantum anomalous Hall state can be realized [2]. This phase is expected to show even more exotic phenomena such as the topological magnetoelectic effect. To realize such state, two types of sample fabrication techniques have been employed up to now: (1) magnetic doping while growing the single crystal or thin film of TI [3], and (2) magnetic impurity deposition on the surface of TI [4]. While method (1) was successful and showed evidence of the TRS violation, no one has succeeded using method (2), which should be a more direct way to examine the interaction between the topological surface states and magnetism. We have previously found another novel technique to induce magnetism into TI, namely the magnetic extension effect [5]. By depositing Mn and Se on $Bi_2Se_3$, we found that Mn and Se are incorporated in the topmost $Bi_2Se_3$ layer and a novel heterostructure $MnBi_2Se_4/Bi_2Se_3$ is formed [5]. This heterostructure with an ordered magnetic Mn single layer showed a clear Dirac cone gap of 85 meV. From magnetic measurements utilizing high-resolution X-ray magnetic circular dichroism (XMCD) at the Mn *L* adsorption edge, it was revealed that the Curie temperature $T_c$ of the system is 15-20K. However, when we fabricated a sandwich structure of $MnBi_2Se_4/n$ quintuple layer (QL) $Bi_2Se_3/MnBi_2Se_4$, which includes two magnetic Mn layers, we found that the $T_c$ was enhanced to 20-25 K for $n$ = 1-7. Thus it is important to measure the electronic structure of the sandwich structure and investigate the origin of the enhancement of $T_c$.

Therefore in this study, we have measured the band dispersion of $MnBi_2Se_4$/7 QL $Bi_2Se_3/MnBi_2Se_4$ sandwich structure by angle-resolved photoemission spectroscopy (ARPES). The band dispersion measured at 10 K is shown in Fig. 1 system. It shows a band structure similar to the heterostructure with a linear dispersion [5] and a quantitative analysis of the energy dispersion curve (EDC) at the Γ point revealed that the gap size was 100 meV. This result showed that there is practically little difference between the hetero and sandwich structures. Further magnetic characterization with XMCD including measurements for nonmagnetic elements (Se or Bi) have given new insights into the magnetic interaction of the two Mn magnetic layers for the sandwich structure. Namely it was revealed that the bulk carriers of the $Bi_2Se_3$ near the Fermi level mediate the magnetic interaction between the two Mn layers [6].

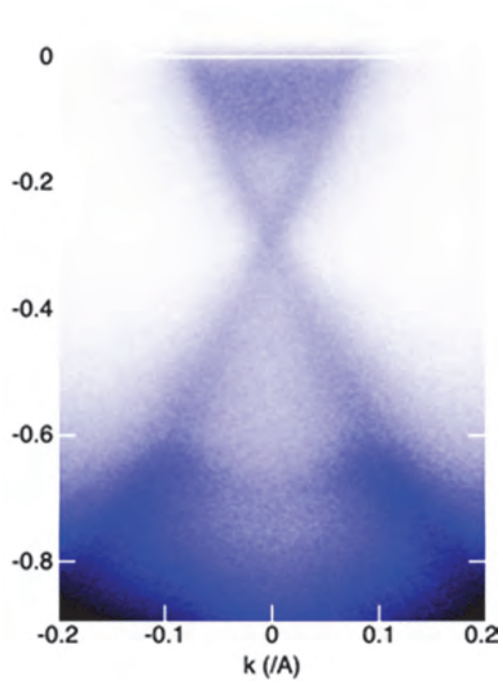


Fig. 1. Band dispersion image of the $MnBi_2Se_4$/7 QL $Bi_2Se_3/MnBi_2Se_4$ sandwich structure measured at 10 K.

[1] M. Hasan and C. Kane, Reviews of Modern Physics **82** (2010) 3045.
[2] X.-L. Qi and S.-C. Zhang, Reviews of Modern Physics **83** (2011) 1057.
[3] For example, C. Z. Chang *et al.,* Science **340** (2013) 167.
[4] For example, M. Ye *et al.,* Physical Review B **85** (2012) 205317.
[5] T. Hirahara *et al.,* Nano Letters **17** (2017) 3493.
[6] R. Fukushima *et al.,* to be published.

BL7U

# Observation of Electronic Structure of $YbCu_2$/Cu(111) Surface Alloy

H. Sugihara[1], T. Nakamura[2,1], Y. Chen[1], K. Tanaka[3] and S. Kimura[2,1,4]

[1]*Department of Physics, Graduate School of Science, Osaka University, Toyonaka 560-0043, Japan*

[2] *Graduate School of Frontier Biosciences, Osaka University, Suita, 565-0871, Japan*

[3]*UVSOR Synchrotron Facility, Institute for Molecular Science, Okazaki 444-8585, Japan*

[4]*Department of Materials Molecular Science, Institute for Molecular Science, Okazaki 444-8585, Japan*

The Kondo coupling between localized *f*-electrons and carriers leads to exotic physical phenomena such as the formation of the heavy-fermion (HF), the emergence of a magnetic quantum critical point, and unconventional superconductivity [1]. Among them, the HF system, in which massive effective carriers appear due to the Kondo effect, has fascinated many researchers [2,3]. On the other hand, the combination of HF system and low-dimensionality strongly modulate the hybridization strength because an order parameter of these systems is much sensitive to dimensionality. In a typical bulk HF compound, $CeIn_3$, for instance, the suppression of the antiferromagnetism and the increase of the carrier's effective mass appear due to the reduction of the dimensionality [4]. In addition, a HF quasicrystal, which has higher dimensionality, has an unconventional quantum criticality [5]. To clarify the relation of the dimensionality to the HF character, we investigate electronic structure of low-dimensional HF materials. Here, we have studied the surface electronic structure of a HF surface alloy, $YbCu_2$/Cu(111), which is a new candidate for the two-dimensional HF system, measured by angle-resolved photoelectron spectroscopy (ARPES).

The clean Cu (111) substrate was prepared by the cycle of $Ar^+$ sputtering and annealing up to 800 K. After checking a sharp and low-background streak electron diffraction pattern, Yb-metal was evaporated by a homemade Knudsen cell, resulting in the observation of fractional order originated from the $YbCu_2$ layer. ARPES measurement was carried out at UVSOR BL7U ($h\nu$ = 21 eV) at temperature of 6 K.

Figure 1 shows the ARPES intensity plot of $YbCu_2$/Cu(111) surface along $\bar{\Gamma}$ - $\bar{K}$ on a surface Brillouin zone of Cu(111). To see the band dispersion above the Fermi level, the ARPES spectra were divided by the Fermi-Dirac distribution function convolved with the instrumental resolution. The flat bands with the binding energy of around 0.2 eV are attributed to the $Yb^{2+}$ $4f_{7/2}$ final state after the photoexcitation process. Several hole bands centered on the $\bar{\Gamma}$ point were observed. The hybridizations between the hole bands and the Yb 4*f* state appears as the modulation of the shapes and intensities. In addition to the hybridization, as shown in Fig. 2, a steep peak, which seems to be a Kondo resonance peak usually observed in HF materials [6], appears near the Fermi level. These results suggest the HF formation in $YbCu_2$/Cu(111).

Further analysis to understand the hybridization between the Yb 4*f* orbital and conductive hole bands and the relation to the dimensionality are in progress.

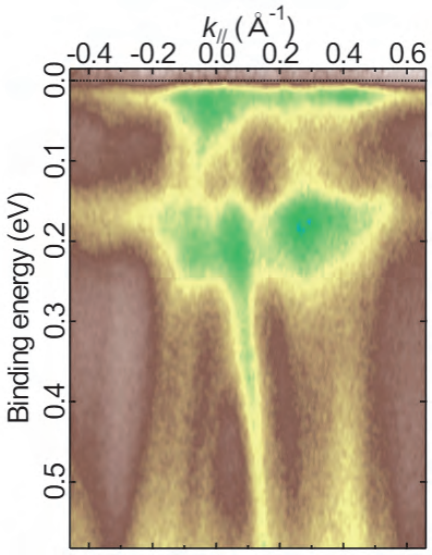


Fig. 1. ARPES band dispersion of $YbCu_2$/Cu(111) surface along $\bar{\Gamma}$-$\bar{K}$ taken at $h\nu$ = 21 eV ($T$ = 6 K). The photoelectron intensities were normalized by Fermi-Dirac distribution function convoluted with the instrumental resolution.

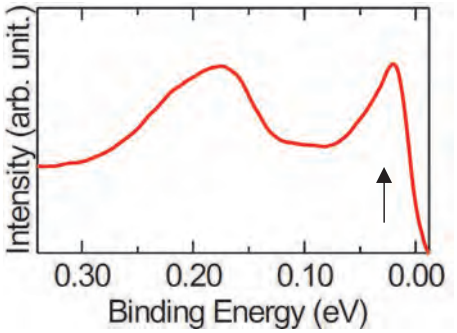


Fig. 2. Angle-integrated photoelectron spectra of $YbCu_2$/Cu(111). The allow indicates the Kondo resonance peak.

[1] C. Pfleiderer, Rev. Mod. Phys. **81** (2009) 1551.
[2] A. C. Hewson, *The Kondo Problem to Heavy Fermions* (Cambridge Univ. Press, Cambridge, 1993).
[3] P. Coleman *et al*, J. Phys.: Condens. Matter **13** (2001) R723.
[4] H. Shishido *et al*., Science **327** (2010) 980.
[5] K. Deguchi *et al.*, Nat. Mater. **11** (2012) 1013.
[6] S. Chatterjee *et al.*, Nat. Commun. **8** (2017) 852.

BL7B

# Electrochemical Attenuated Total Reflectance Ultraviolet (EC-ATR-UV) Spectroscopy Applied for Organic Semiconductor / Ionic Liquids Interface

I. Tanabe, Y. Hanamori and K. Fukui

*Department of Materials Engineering Science, Graduate School of Engineering Science, Osaka University, Toyonaka 560-8531, Japan*

Electric double-layer organic field-effect transistors (EDL-OFETs) have attracted much attention because of their significantly low operation voltage (<1 V) compared to conventional $SiO_2$-gated OFETs (>10 V). In EDL-OFETs, a high electric field is generated in the EDL that accumulates in the interfacial region between the organic semiconductor and electrolyte, resulting in a low operation voltage. Therefore, the organic semiconductor/electrolyte interface is especially important. Recently, we developed a new spectroscopic system, namely electrochemical- attenuated total reflectance (EC-ATR) ultraviolet-visible spectroscopy, which can access the interfacial area [1,2].

In this study, ionic liquid gated organic field-effect transistors (IL-gated OFETs) were fabricated on the ATR prism (Fig. 1). Two-layer single crystalline film of $C_9$-DNBDT-NW was used as an organic semiconductor, and two kinds of ionic liquids ([EMIM][FSA] and [TMPA][TFSA]) were cast on the film. Au films were evaporated to a thickness as the source and drain electrodes (working electrodes) on both sides of the ATR prism, and a Pt coil and a Pt wire were placed in the ionic liquids as pseudo counter and reference (gate) electrodes, respectively. In our previous study [2], in response to the applied gate voltage, the spectral peaks of the organic semiconductor shifted and bleached. This was correlated with the drain current.

The fabricated IL-gated OFETs on the ATR prism was put on the sample chamber in BL7B at UVSOR. The light from UVSOR had one important advantage; polarization direction control. That is to say, by changing the placing direction of the ATR prism to the incident light, the polarized direction to the sample can be controlled. While our previous study used a halogen lamp as the light source, which was unpolarized, the synchrotron radiation is innately polarized. in the UV region, especially in the deep-UV (<300 nm) region, the preparation of a polarizer is difficult, and thus, the polarized light generated from the synchrotron is highly useful.

Figure 2 shows the ATR spectra of $C_9$-DNBDT-NW on the sapphire prism measured in BL7B at UVSOR. While the *s*-polarized incident light gave distinct peaks in the 200-500 nm range (Fig. 2 (a)), *p*-polarized incident light did not (Fig. 2 (b)). This is because the $C_9$-DNBDT-NW film on the ATR prism was well packed, and shows strong polarized dependence.

These peaks could be assigned by quantum chemical calculations, and they verified depending on the applied voltage [2]. In addition, EC-ATR-UV spectroscopy could measure the absorbance due to the ionic liquids near the surface of the $C_9$-DNBDT-NW film because of the short penetration depth (< 50 nm) and the strong ionic liquids' absorbance of the light in the UV region, which was a unique point of the new technique. Therefore, we are trying spectral measurements of both organic films and ionic liquids during device operations using the polarized light from BL7B. It will reveal orientations of interfacial ionic liquids and their behaviors under electrochemical environment. Additionally, the interactions between the organic semiconductor film and ionic liquids will be investigated, leading to the mechanism research and improvement of the high performance EDL-OFETs.

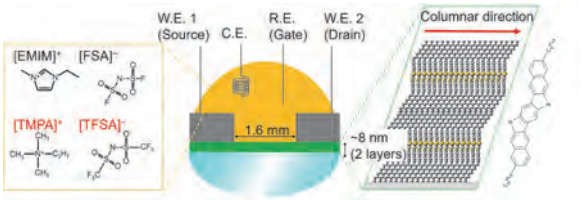


Fig. 1. Schematics of EDL-OFET fabricated on ATR prism.

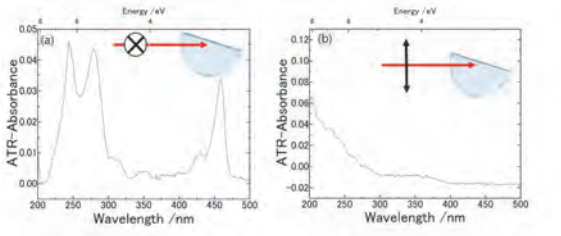


Fig. 2. Polarization dependence of ATR spectra of $C_9$-DNBDT-NW on a sapphire prism.

[1] I. Tanabe, A. Suyama, T. Sato and K. Fukui, Anal. Chem. **91** (2019) 3436.
[2] I. Tanabe, I. Imoto, D. Okaue, M. Imai, S. Kumagai, T. Makita, M. Mitani, T. Okamoto, J. Takeya and K. Fukui, Commun. Chem. **4** (2021) 88.

# UVSOR User 6

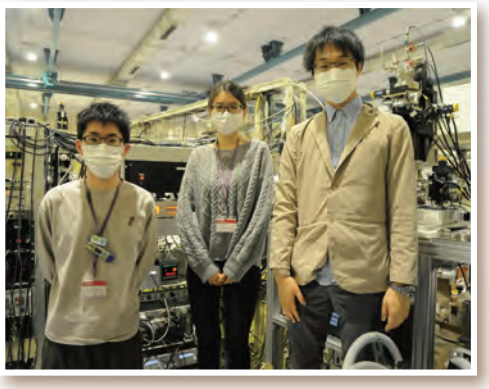

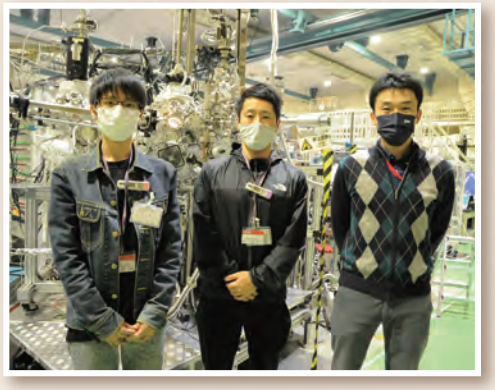

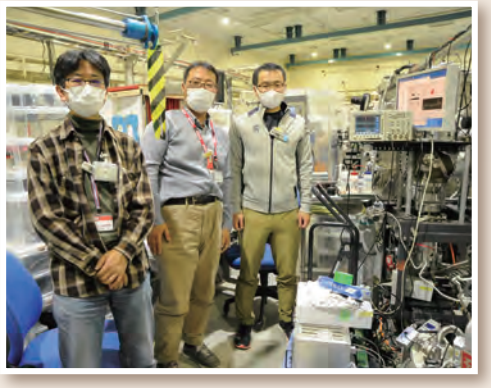

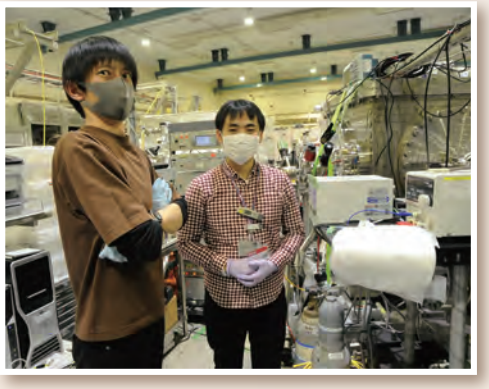

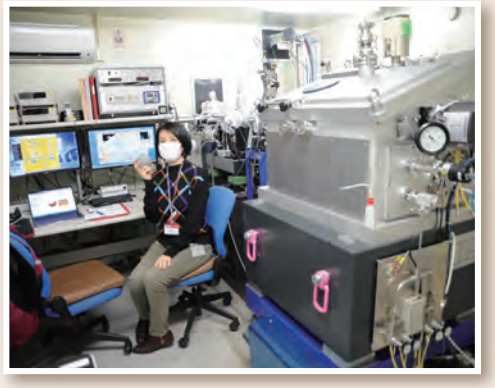

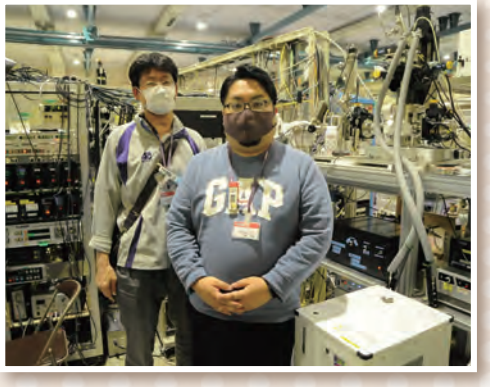

# UVSOR User 7